

Research Article

Open Access



Simultaneously enhancing moisture and mechanical stability of flexible perovskite solar cells via a polyimide interfacial layer

Zhuoxi Li¹, Xiangyu Kong¹, Yue Jiang^{1,2}, Xubing Lu¹, Xinseng Gao¹, Chaoliang Tan³, Yiwang Chen⁴, Guofu Zhou⁵, Jun-Ming Liu⁶, Jinwei Gao¹

¹Institute for Advanced Materials and Guangdong Provincial Key Laboratory of Optical Information Materials and Technology, South China Academy of Advanced Optoelectronics, South China Normal University, Guangzhou 510006, Guangdong, China.

²Key Lab of Functional Molecular Engineering of Guangdong Province, South China University of Technology, Guangzhou 510640, Guangdong, China.

³Department of Electrical Engineering, City University of Hong Kong, Kowloon, Hong Kong 999077, China.

⁴Institute of Polymers and Energy Chemistry, College of Chemistry, Nanchang University, Nanchang 330031, Jiangxi, China.

⁵Guangdong Provincial Key Laboratory of Optical Information Materials and Technology & Institute of Electronic Paper Displays, South China Academy of Advanced Optoelectronics, South China Normal University, Guangzhou 510006, Guangdong, China.

⁶Laboratory of Solid-State Microstructures, Nanjing University, Nanjing 210093, Jiangsu, China.

Correspondence to: Prof. Jinwei Gao, Institute for Advanced Materials and Guangdong Provincial Key Laboratory of Optical Information Materials and Technology, South China Academy of Advanced Optoelectronics, South China Normal University, Guangzhou 510006, Guangdong, China. E-mail: gaojinwei@m.scnu.edu.cn; Dr. Yue Jiang, Institute for Advanced Materials and Guangdong Provincial Key Laboratory of Optical Information Materials and Technology, South China Academy of Advanced Optoelectronics, South China Normal University, Guangzhou 510006, Guangdong, China. E-mail: yuejiang@m.scnu.edu.cn

How to cite this article: Li Z, Kong X, Jiang Y, Lu X, Gao X, Tan C, Chen Y, Zhou G, Liu JM, Gao J. Simultaneously enhancing moisture and mechanical stability of flexible perovskite solar cells via a polyimide interfacial layer. *Soft Sci* 2021;1:4. <https://dx.doi.org/10.20517/ss.2021.06>

Received: 5 Jul 2021 **First Decision:** 14 Jul 2021 **Revised:** 29 Jul 2021 **Accepted:** 30 Jul 2021 **First online:** 31 Jul 2021

Academic Editor: Zhifeng Ren **Copy Editor:** Xi-Jun Chen **Production Editor:** Xi-Jun Chen

Abstract

Perovskite solar cells (PSCs) have aroused tremendous attention due to the high power conversion efficiency (PCE) and flexibility of the organic-inorganic hybrid perovskite films. However, the commercialization of perovskite solar cells is still impeded due to the instability issue induced by moisture and mechanical stress. Herein, we introduce soluble hydrophobic polyimide (PI) as an interfacial layer on top of the perovskite film to block the infiltration of moisture into the perovskite film. The MAPbI₃-based solar cell with the insertion of PI layer exhibited an impressive stability, maintaining 87% of the initial PCE even after exposing to 50% relative humidity for 550 h and presenting a decent PCE of 21.22% due to its ability to extract holes and reduce trap-assisted recombination. Moreover, the high tolerance of PI to the mechanical stress gives a more stable flexibility to the PSCs under



© The Author(s) 2021. **Open Access** This article is licensed under a Creative Commons Attribution 4.0 International License (<https://creativecommons.org/licenses/by/4.0/>), which permits unrestricted use, sharing, adaptation, distribution and reproduction in any medium or format, for any purpose, even commercially, as long as you give appropriate credit to the original author(s) and the source, provide a link to the Creative Commons license, and indicate if changes were made.



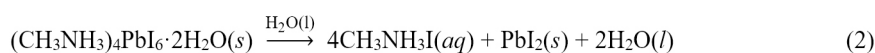
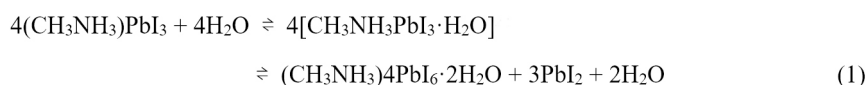
constant bending.

Keywords: Stability, hydrophobic, charge extraction, perovskite solar cells

INTRODUCTION

Organic-inorganic hybrid metal halide perovskite (OMHP) materials, as one of the most promising light-harvesting materials for photovoltaic devices, have been widely applied in perovskite solar cells (PSCs) by their virtues of outstanding optoelectronic properties and easy fabricating process^[1-3]. Further, the flexibility of PSCs can help their integration with other power sources in wearable electronics^[4]. To date, the certified power conversion efficiency (PCE) has reached 25.5%^[5-7], steadily approaching the performance of monocrystalline silicon solar cells. Nevertheless, the instabilities of OMHP caused by heat, oxygen, moisture, or mechanical stress tremendously hinder the commercialization of PSCs^[8-10].

Considering the ionic interaction in OMHP, water is the dominating factor during the degradation process at ambient atmosphere. As for methylammonium lead triiodide (MAPbI₃), its exposure to moisture would quickly and reversibly transform the original perovskite phase into intermediate monohydrates or even dihydrates byproducts, which would further irreversibly decompose into CH₃NH₃I and PbI₂, as illustrated in Equations (1) and (2)^[11].



To prevent the perovskite from being destroyed by moisture, a possible solution is to utilize hydrophobic hole-transporting materials (HTMs). For example, Xie *et al.*^[12] introduced the hydrophobic and dopant-free Co-Ni bimetal-doped carbon aerogels simultaneously as HTM and electrode, remarkably improving the long-term stability of perovskite: 86% of the initial efficiency was maintained even after 1296 h exposure in air. Similarly, Zheng *et al.*^[13] and Li *et al.*^[14] adopted the hydrophobic 2D perovskite materials as HTM and thus enhanced the moisture resistance of perovskite. Despite their excellent moisture stability, these stable devices always suffered from low efficiencies compared with the devices based on spiro-OMeTAD HTM. Instead, when a small amount of 2D perovskite is added into 3D perovskite, both moisture stability and photoelectric performance can be improved^[15,16].

Another important strategy is to apply effective water barrier polymer layers to encapsulate the perovskite film. Kim *et al.*^[17] demonstrated that hygroscopic polyethylene oxide can absorb water before the perovskite layer, preventing water from permeating into the perovskite film. On the other hand, a hydrophobic polymer layer can also protect perovskite from water penetration. Zhang's group deposited polystyrene on top of the perovskite layer, maintaining 73% of the initial PCE after 60 h in 80% humidity^[18]. These approaches show the feasibility of employing a polymer as a functional layer to enhance the stability of perovskite films. Polyimide (PI) is a kind of multifunctional engineering materials with a high tolerance to temperature and mechanical stress. PI has been used as an additive to enhance the photovoltaic performance of PSCs^[19] and as foldable substrates in flexible devices^[20,21]. Nevertheless, few studies apply PI as an interfacial layer.

We introduced a soluble hydrophobic polymer, PI, by a spin-coating deposition method on top of perovskite films. By employing PI as the interfacial layer, a PCE of 21.22% was achieved based on MAPbI₃, which could maintain 87% of the original PCE after more than 550 h aging in 50% relative humidity (RH) and 72% of the original PCE after 2500 cycles of bending. Further detailed studies showed that PI layer not only exhibits an excellent ability in extracting holes but also passivates the surface traps.

EXPERIMENTAL

Material and solvent

Methylammonium iodide (MAI, 99.5%) was purchased from Xi'an Polymer Light Technology Corp. Lead iodide (PbI₂, 99.999%) and 2,2',7,7'-tetrakis(N,N-di-p-methoxyphenylamine)-9,9-spirobifluorene (spiro-OMeTAD, 99.8%) were purchased from Yingkou Libra New Energy Technology Co., Ltd. The aqueous dispersion of PEDOT:PSS (AI 4083) was obtained from Shanghai MaterWin New Materials Co., Ltd. Bis(trifluoromethanesulfonyl)imide (Li-TFSI, 99.5%), tert-butylpyridine (t-BP, 98%), and Tin(II) chloride dihydrate (SnCl₂·2H₂O, 98%) were purchased from Sigma-Aldrich. A soluble polyimide (PI, 5 wt% in N-Methylpyrrolidone) was obtained from ShenZhen Dalton Electronic Material Co., Ltd. As for solvent, dimethyl formamide (DMF, 99.8%), dimethyl sulfoxide (DMSO, 99.9%), chlorobenzene (CB, 99.8%), acetonitrile (99.8%), and butanol (99.8%) were purchased from Sigma-Aldrich and used without further purification. FTO glasses (FTO, 7 Ω per square) were purchased from Advanced Election Technology Co., Ltd.

Solution preparation

The SnO₂ nanocrystalline (NC) solution was prepared by our previous method^[22]. Typically, the SnCl₂·2H₂O solution (0.1 M) was prepared by dissolving SnCl₂·2H₂O separately in 20 mL butanol containing 2 mL water in a flask. Then, the solution was separately stirred at room temperature for 10 min. To synthesize colloidal SnO₂ NC, the SnCl₂·2H₂O solution was refluxed at 110 °C for 2-4 h with an open refluxing apparatus.

The perovskite precursor was prepared by dissolving 922 mg PbI₂ and 318 mg MAI into 1.6 mL mixed solvent of DMF and DMSO (7:3 *v/v*). Spiro-OMeTAD solution was prepared by dissolving 72 mg spiro-OMeTAD into 1 mL CB, with the dopant of 17.5 μL Li-TFSI solution (520 mg in 1 mL acetonitrile) and 28.8 μL t-BP.

Perovskite solar cells fabrication

The FTO substrates were sequentially ultrasonically cleaned with detergent, deionized water, and isopropanol for 15 min, respectively. Before spin-coating SnO₂ ETLs, the FTO substrates were further cleaned by UV-ozone for 15 min. Then, the SnO₂ NC solution was dropped on the FTO substrates and spin-coated at 500 rpm for 3 s and 3000 rpm for 30 s, followed by thermal annealing at 150 °C for 1 h. After the substrates cooled down, a 15 min UV-ozone treatment was operated again. Then, all substrates were transfer into a glovebox filled with N₂ atmosphere to complete the subsequent process. The perovskite precursor solution was spin-coated on SnO₂ layer at 500 rpm for 3 s and 4000 rpm for 30 s. Then, 400 μL CB as antisolvent were dripped onto the perovskite film 21 s prior to the end of the second spinning program. Afterward, the perovskite film was annealed on hotplate at 100 °C for 10 min. PI solution (0.5, 1.0, 1.5, and 2.0 wt% in CB) was spin-coated at 500 rpm for 3 s and 4000 rpm for 30 s, followed by 20 min annealing treatment at 100 °C. When it cooled down, spiro-OMeTAD solution was spin-coated upon the perovskite film at 500 rpm for 3 s and 3000 rpm for 30 s. Finally, the Ag electrode was thermally evaporated on top of the device under high vacuum condition (< 5 × 10⁻⁴ Pa). The active area of all devices was 0.07 cm² defined by a metal mask.

Characterization

The surface and cross-section morphologies of perovskite and PSCs devices were investigated by FE-SEM (ZEISS Ultra-55). The ultraviolet and visible spectrophotometry (UV-vis) absorption spectra of perovskite film were measured by SHIMADZU UV-2700 in the wavelength range of 450–850 nm. The surface roughness of the perovskite film was obtained from atomic force microscope (AFM) (Asylum Research, Cypher). The water contact angle of the perovskite surface was measured by contact angle tester (Dataphysics OCA20, German). Ultraviolet photoelectron spectroscopy was performed on SHIMADZU AXIS SUPRA. The Fourier transform infrared (FTIR) spectrum was conducted on Bruker Vertex 70. The current-voltage (*J*-*V*) curves of the non-encapsulated solar cells were measured by Keithley 2400 by forward scan (1.2 to -0.2 V) with a scanning rate of 50 mV/s (voltage step of 10 mV and delay time of 50 ms) in a glovebox under AM 1.5 G illuminations (100 mW·cm⁻²) from a solar simulator (Newport, 91160), which was calibrated using a standard silicon solar cell device by the NREL. Steady-state photoluminescence (PL) spectra were measured under an excitation wavelength of 460 nm by using Lenggung F97pro Fluorescence Spectrophotometer. Time-resolved photoluminescence (TRPL) spectra were recorded by a spectrofluorometer (Edinburgh FLS9800) under a 450 nm excitation. Electrochemical impedance spectroscopy (EIS) was studied on an electrochemical workstation (CHI660) from 1 MHz to 1 Hz, biased at 0.2 V in the dark. X-ray diffraction (XRD) (PANalytical X'Pert PRO) was performed with Cu K α radiation under operating conditions of 40 kV and 40 mA. The space charge limited current (SCLC) characteristic of the devices was measured using a Keithley 2400 in the dark. According to SCLC theory, the defect (trap) density (n_{trap}) can be estimated as follows: $n_{\text{trap}} = (2\epsilon\epsilon_0 V_{\text{TFL}})/(eL^2)$, where L , ϵ , ϵ_0 , and e are the thickness of the perovskite film (ca. 530 nm), dielectric constant of the material, permittivity of vacuum, and electronic charge, respectively. The external quantum efficiency (EQE) measurements of devices were carried out using QE-C system (Taiwan, Enlitech) in a wavelength range of 300–900 nm.

RESULTS AND DISCUSSION

The concentration of the PI was optimized by characterizing the morphology of PI films on top of the perovskite with the top-view scanning electron microscopy (SEM), as shown in [Figure 1A-E](#). The pristine perovskite film [[Figure 1A](#)] shows a compact surface with grain sizes ranging from 200 to 600 nm. After combining the PI layer [[Figure 1B-E](#)], the morphologies of perovskite films have no apparent changes compared with that of pristine film. Specially, PI at lower concentration (0.5 wt%) gives a relatively flat and continuous morphology, which was also confirmed by the AFM, as illustrated in [Supplementary Figure 1](#). The water contact angles were largely changed after the inset of the PI layer on top of the perovskite films, as shown in [Figure 1F-J](#). Due to the high hydrophobicity of PI, the contact angle of perovskite was sharply increased from 56.9° (pristine) to 95.3° (PI layer at the concentration of 2 wt%) upon the insertion of PI interfaces, providing the possibility of efficient inhibiting of moisture degradation^[23]. By measuring the ultraviolet photoelectron spectroscopy curves of the perovskite films with and without PI, the energy level diagram of the PSC could be drawn [[Supplementary Figure 2](#)]. Due to the thin thickness of PI (~10 nm, as shown in [Supplementary Figure 3](#)), holes from the value band maximal of perovskite can tunnel to spiro-OMeTAD^[24,25]. The FTIR spectrum of pure PI is presented in [Supplementary Figure 4](#), showing the characteristic band peaks of the imide carbonyl were 1779 cm⁻¹ (asymmetric C=O, stretching), 1721 cm⁻¹ (symmetric C=O, stretching), and 1362 cm⁻¹ (C-N, stretching)^[26,27].

Planar PSCs with configuration of FTO/SnO₂/MAPbI₃/PI/spiro-OMeTAD/Ag were fabricated, with the thickness of SnO₂, MAPbI₃, spiro-OMeTAD, and Ag being about 30, 300, 140, and 80 nm, respectively, as shown in the cross-sectional SEM image [[Supplementary Figure 5](#)]. These PSCs were then measured under an irradiation intensity of 100 mW/cm² (AM 1.5 G solar spectrum), and the current density-voltage curves (*J*-*V*) along with the related parameters are illustrated in [Figure 2A](#). As the concentration of PI increased from 0 wt% to 2 wt%, the corresponding PCE of the devices was first enhanced from 20.72% (V_{OC} of 1.17 V,

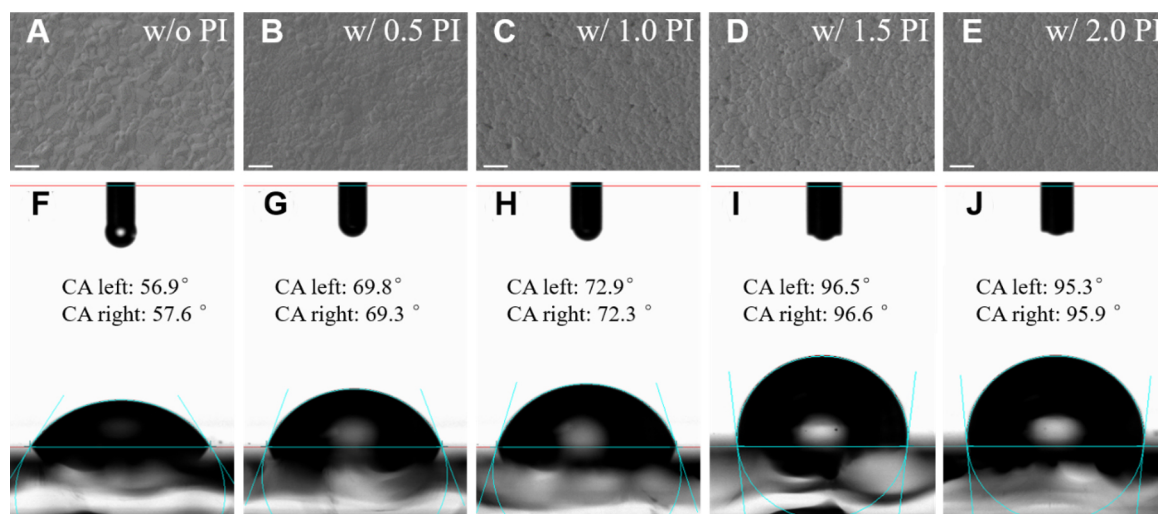


Figure 1. Top-view SEM images of pristine perovskite films (A). Top-view SEM images of perovskite films modified by PI solution with different concentrations: (B) 0.5 wt%; (C) 1.0 wt%; (D) 1.5 wt%; and (E) 2.0 wt%. The corresponding water contact angles based on the above perovskite films: (F) for (A); (G) for (B); (H) for (C); (I) for (D); and (J) for (E). SEM: Scanning electron microscopy. PI: polyimide.

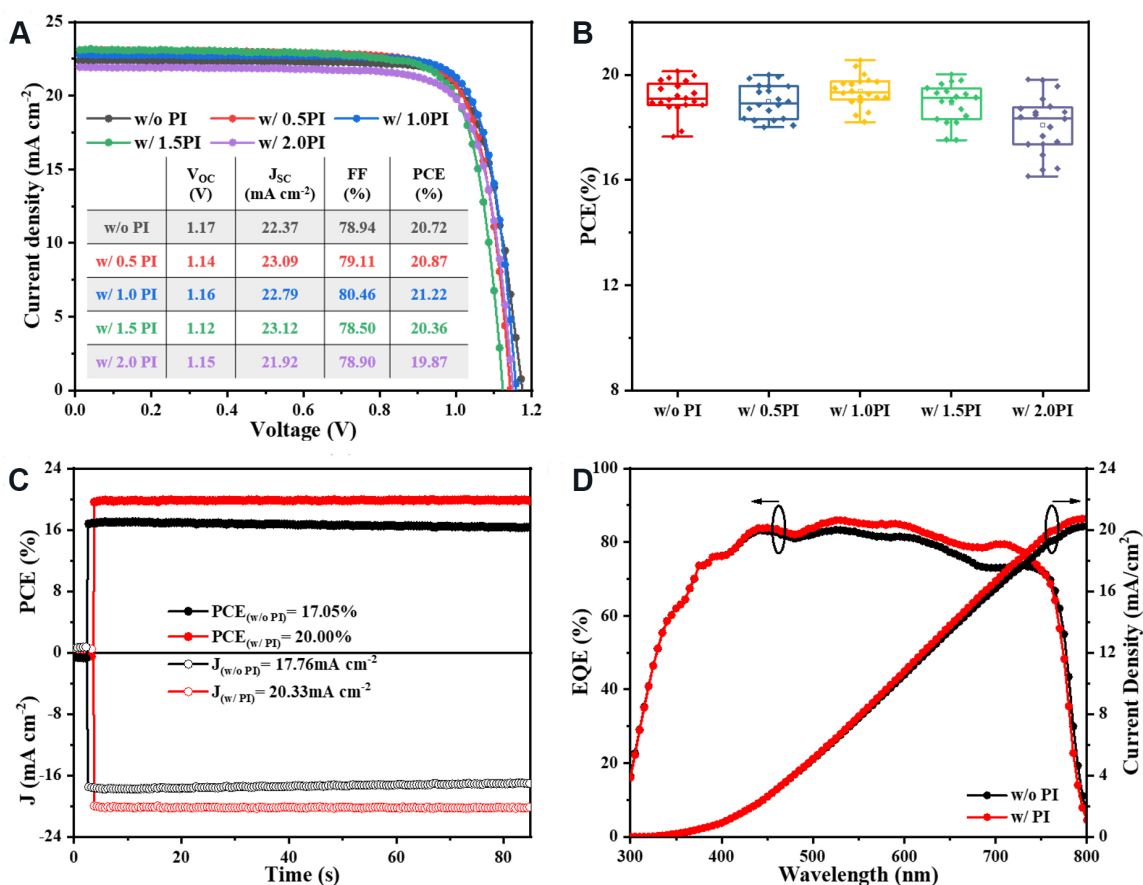


Figure 2. (A) J-V curves and (B) the PCE statistical distributions of 20 devices with different concentrations of PI. (C) The steady-state photocurrent measurements at maximum power point. (D) EQE spectra for the devices with (w/) and without (w/o) PI. PCE: High power conversion efficiency; EQE: external quantum efficiency; PI: polyimide.

J_{SC} of 22.37 mA/cm², and FF of 78.94%) at 0 wt% to 21.22% (V_{OC} of 1.16 V, J_{SC} of 22.79 mA/cm², and FF of 80.46%) at 1 wt%, while the PCE decreased to 19.87% (V_{OC} of 1.15 V, J_{SC} of 21.92 mA/cm², and FF of 78.90%) when 2 wt% of PI was used, which is considered to have arisen by the charge blocking effect of thick PI films^[28].

The statistical PCE distribution of 20 independent devices fabricated from PI solution shown in [Figure 2B](#) suggests the same trend as the J - V curves. Besides, the devices based on 1.0 wt% PI exhibit the smallest variation and the best reproducibility. Therefore, it was chosen to compare with the PI-free device to the device with PI in the subsequent characterization, denoted as w/o PI and w/ PI, respectively.

To further confirm the values obtained from J - V curves, steady-state PCE was recorded over 85 s under the maximum power point voltage (0.98 and 0.96 V for devices w/ PI and w/o PI), as shown in [Figure 2C](#), giving a PCE of 20.00% with the stabilized J_{SC} of 20.33 mA/cm² and a PCE of 17.05% with the stabilized J_{SC} of 17.76 mA/cm². Furthermore, the integrated J_{SC} from EQE curves of devices w/ PI and w/o PI in [Figure 2D](#) are 20.76 and 20.29 mA/cm², respectively, which agrees well with the J - V curves.

The dynamics of photo-excited carriers was investigated to understand the origin of the PCE enhancement after inserting this high-dielectric PI by PL and TRPL measurement, as shown in [Figure 3A](#). A strong luminescence peak at 780 nm was observed, which was significantly decreased upon the insertion of PI interface, demonstrating the improved charge transfer efficiency. In addition, the PL lifetime was obtained by fitting the TRPL [[Figure 3B](#)] spectra with a two-exponential decay model: $I(t) = A_1 \exp(-t/\tau_1) + A_2 \exp(-t/\tau_2) + I_0$. The fast decay lifetimes (τ_1) represent the nonradiative recombination induced by the trapping process when the charge goes through the perovskite surface, and the slow decay lifetimes (τ_2) are related to the radiative recombination process occurring in the bulk perovskite^[29-31]. The fitted parameters are summarized in [Supplementary Table 1](#). In this case, the average charge lifetime (τ_{avg}) was estimated to be 220.9 and 32.1 ns for devices w/o PI and w/ PI, respectively, apparently confirming that the PI layer is greatly beneficial for the hole-extraction process^[32] and contributes to the increase of the FF.

Subsequently, to assess the hole-trap density at the perovskite/spiro-OMeTAD interfaces modified by PI layer, the SCLC method was conducted based on the hole-only devices, FTO/PEDOT:PSS/perovskite/with or without PI layer/spiro-OMeTAD/Ag. As shown in [Figure 3C](#), the ohmic conducting region at lower voltage and trap-filled limited (TFL) region at higher voltage intersect at one point, where its corresponding voltage is the trap-filled limit voltage (V_{TFL})^[33], which is reported positively correlated with the trap density (n_{traps})^[34]. In [Figure 3C](#), the V_{TFL} of devices w/o PI and w/ PI was measured to be 0.84 and 0.77 V, corresponding to a n_{traps} of 9.31×10^{15} and 8.22×10^{15} cm⁻³, respectively. Thus, we could conclude that inserting PI is an effective strategy for the suppression of traps, further favoring the efficient charge transfer at the perovskite/spiro-OMeTAD interfaces.

Moreover, from the Nyquist plots of PSCs in [Figure 3D](#), obtained by EIS measurement in the dark, the semi-circle of the device w/ PI exhibits a smaller radius in the high frequency region, which demonstrates a lower charge transfer resistance (R_{ct}). Simultaneously, the radius of its semi-circle in the low frequency region associated with the recombination resistance (R_{rec})^[35] is bigger than that of device w/o PI, consistent with the conclusion that the trap was mitigated by the PI interfaces.

Finally, the influence of PI interfaces on the moisture and mechanical stability is shown in [Figure 4](#). Firstly, MAPbI₃ was deposited on the FTO substrate, followed by the deposition of the PI polymer. After a certain exposure time under high RH of 75% at 25 °C, the degree of degradation could be observed from the UV-vis

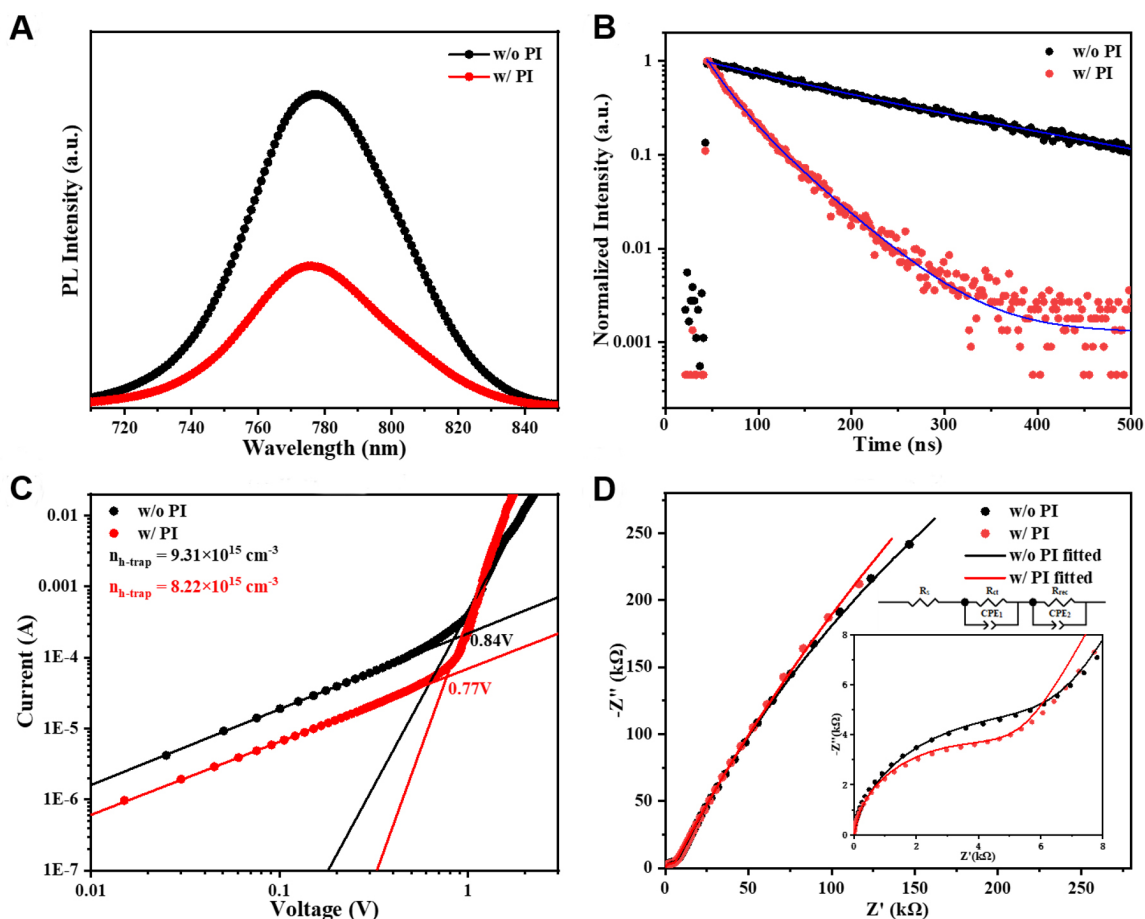


Figure 3. (A) PL spectra and (B) TRPL decay curves for the devices with (w/) and without (w/o) PI. (C) The dark current-voltage curves for hole-only devices with (w/) and without (w/o) PI. (D) Nyquist plots of the devices with (w/) and without (w/o) PI, measured in the dark. TRPL: Time-resolved photoluminescence; PI: polyimide; PL: photoluminescence.

absorption curve, as shown in [Figure 4A](#). Both films showed a similar high absorbance on the first day, indicating that the introduction of PI layer has little effect on light absorption. After six days of exposure, the absorbance of the perovskite film w/o PI dropped sharply, while the PI-modified film gave little change. Simultaneously, XRD measurement was conducted to trace the phase transition of perovskite films. [Figure 4B](#) shows that the fresh w/o PI and w/ PI films presented main diffraction peaks of perovskite at 14.12° . However, in the spectra of aged perovskite film w/o PI (75% RH for four days), obvious peaks at 12.57° , 10.17° , and 8.40° , ascribed to PbI_2 and monohydrate perovskite, were detected^[11,36], forming a sharp contrast with the film w/ PI. Thereby, it is considered that the insertion of the PI layer indeed protects the perovskite film from fast moisture intrusion in high-humidity environments.

The long-term stability of PSCs in ambient condition was evaluated by monitoring the PCE of the devices without any encapsulation under 50% RH at 25°C . As shown in [Figure 4C](#), with PI treatment, the devices maintained 87% of their original PCE after aging over 550 h, whereas the PCE of the pristine perovskite films dropped to 58% of initial PCE. The insert figures show the optical photos of perovskite films stored in the same condition, where transparent hydrate can be found in the PI-free film after aging.

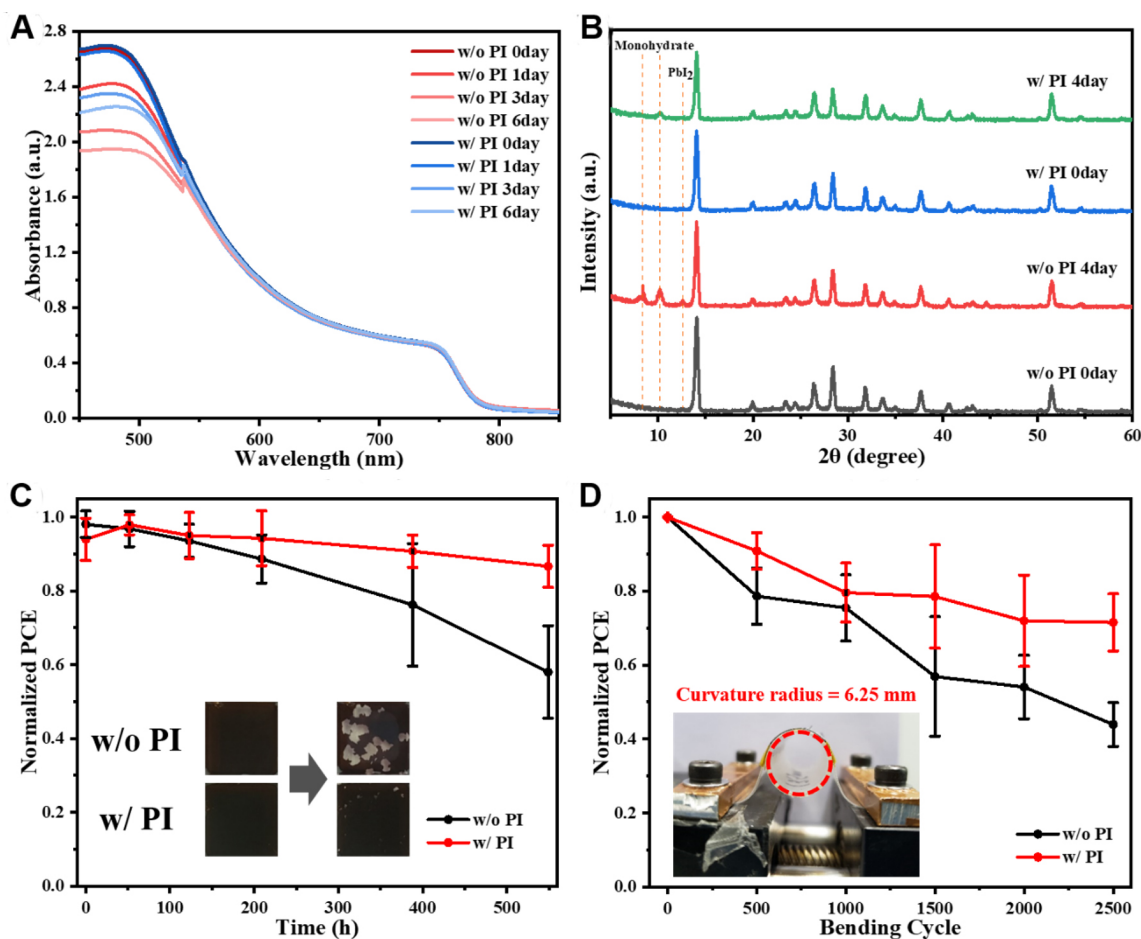


Figure 4. (A) Variations of the UV-vis absorption and (B) XRD measurement of perovskite without and with PI under an RH of 75% at 25 °C in dark conditions with respect to the exposure duration. (C) Long-term stability of the six corresponding PSCs under an RH of 50% at 25 °C in dark conditions. The inserts are optical photographs. (D) Normalized average PCE of 10 PSCs as a function of stretching cycles under a curvature radius of 6.25 mm. The inset shows the photograph of the flexible device under curvature. XRD: X-ray diffraction RH: relative humidity; PSCs: perovskite solar cells; PI: polyimide.

Aiming to validate the mechanical stability of the devices, the flexible PSCs were fabricated based on polyethylene naphthalate (PEN)/ITO substrate with or without PI, which showed a PCE of 17.52% and 16.90%, respectively [Supplementary Figure 6]. Figure 4D shows the normalized average PCE versus bending cycle under a curvature radius of 6.25 mm. The PI-modified devices exhibit remarkable stretching tolerance, maintaining 72% of the original PCE after 2500 cycles, while the PSCs without PI only gave 44% of the pristine PCE, possibly due to the formation of crack on the perovskite film^[37]. Supplementary Table 2 shows a comparison of the moisture stability and mechanical stability of PSCs assisted by polymers, where our work shows outstanding moisture and mechanical stability. Moreover, our PI presents a simultaneous enhancement of both aspects. Thus, it is concluded that the high tolerance of mechanical stress of PI on top of perovskite could take part in the applied mechanical extrusion, giving rise to the mitigated influence of external mechanical stress.

CONCLUSIONS

In summary, we introduced a soluble PI as an interfacial layer to enhance the moisture and mechanical resistance. Further investigations manifested that the PI layer not only extracted holes but also reduced trap-assisted recombination at the interface, achieving a PCE of 21.22% in MAPbI₃-based PSCs. Most

importantly, at 50% RH, the devices with PI layer maintained 87% of the initial PCE after aging over 550 h, far superior to the pristine solar cells. Moreover, PI insertion enhanced the device tolerance against the external mechanical stress, providing an effective strategy to improve the stability of flexible PSCs.

DECLARATIONS

Acknowledgments

The authors gratefully acknowledge the funding support by NSFC Funds (U1801256, 51803064), Science and Technology Programs of Guangzhou (2019050001, 202002030130), International Cooperation Projects of Guangdong Province (2020A0505100054), Guangdong Provincial Key Laboratory of Optical Information Materials and Technology (2017B030301007), and Collaborative Research Fund (CRF C7018-20GF) of Hong Kong Research Grants Council. We also thank the support from the Guangdong Provincial Engineering Technology Research Center for Transparent Conductive Materials, and the Open Fund of the Key Laboratory of Functional Molecular Engineering of Guangdong Province (2018kfx, South China University of Technology).

Authors' contributions

Contributions to conception and design of the study: Li Z, Jiang Y, Gao J

Data analysis and interpretation and data acquisition: Li Z, Kong X, Jiang Y, Gao J, Chen Y, Tan C

Administrative, technical, and material support: Gao J, Gao X, Lu X, Liu JM, Zhou G

Manuscript writing: Li Z, Jiang Y, Gao J

Availability of data and materials

Not applicable.

Financial support and sponsorship

National Natural Science Foundation of China.

Conflicts of interest

All authors declared that there are no conflicts of interest.

Ethical approval and consent to participate

Not applicable.

Consent for publication

Not applicable.

Copyright

© The Author(s) 2021.

REFERENCES

1. Zhang F, Zhu K. Additive engineering for efficient and stable perovskite solar cells. *Adv Energy Mater* 2020;10:1902579. [DOI](#)
2. Chen J, Park N. Materials and methods for interface engineering toward stable and efficient perovskite solar cells. *ACS Energy Lett* 2020;5:2742-86. [DOI](#)
3. Ran C, Xu J, Gao W, Huang C, Dou S. Defects in metal triiodide perovskite materials towards high-performance solar cells: origin, impact, characterization, and engineering. *Chem Soc Rev* 2018;47:4581-610. [DOI](#) [PubMed](#)
4. Zhao J, Xu Z, Zhou Z, et al. A safe flexible self-powered wristband system by integrating defective MnO_{2-x} nanosheet-based Zinc-Ion batteries with perovskite solar cells. *ACS Nano* 2021;15:10597-608. [DOI](#) [PubMed](#)
5. National Renewable Energy Laboratory USA, Best research-cell efficiencies. Available from: <https://www.nrel.gov/pv/cell-efficiency.html>. [Last accessed on 9 Aug 2021].
6. Jiang Q, Zhao Y, Zhang X, et al. Surface passivation of perovskite film for efficient solar cells. *Nat Photonics* 2019;13:460-6. [DOI](#) [PubMed](#)
7. Yoo JJ, Seo G, Chua MR, et al. Efficient perovskite solar cells via improved carrier management. *Nature* 2021;590:587-93. [DOI](#)

[PubMed](#)

8. Wang R, Mujahid M, Duan Y, Wang Z, Xue J, Yang Y. A review of perovskites solar cell stability. *Adv Funct Mater* 2019;29:1808843. [DOI](#)
9. Niu T, Lu J, Munir R, et al. Stable high-performance perovskite solar cells via grain boundary passivation. *Adv Mater* 2018;30:e1706576. [DOI](#) [PubMed](#)
10. Choi K, Lee J, Kim HI, et al. Thermally stable, planar hybrid perovskite solar cells with high efficiency. *Energy Environ Sci* 2018;11:3238-47. [DOI](#)
11. Leguy AMA, Hu Y, Campoy-quiles M, et al. Reversible hydration of $\text{CH}_3\text{NH}_3\text{PbI}_3$ in films, single crystals, and solar cells. *Chem Mater* 2015;27:3397-407. [DOI](#)
12. Xie Y, Cheng J, Liu H, et al. Co-Ni alloy@carbon aerogels for improving the efficiency and air stability of perovskite solar cells and its hysteresis mechanism. *Carbon* 2019;154:322-9. [DOI](#)
13. Zheng H, Liu G, Zhu L, et al. The effect of hydrophobicity of ammonium salts on stability of quasi-2D perovskite materials in moist condition. *Adv Energy Mater* 2018;8:1800051. [DOI](#)
14. Li F, Zhang J, Jo S, et al. Vertical orientated Dion-Jacobson quasi-2D perovskite film with improved photovoltaic performance and stability. *Small Methods* 2020;4:1900831. [DOI](#)
15. Wang Z, Lin Q, Chmiel FP, Sakai N, Herz LM, Snaith HJ. Efficient ambient-air-stable solar cells with 2D-3D heterostructured butylammonium-caesium-formamidinium lead halide perovskites. *Nat Energy* 2017;2:17135. [DOI](#)
16. Zhang T, Dar MI, Li G, et al. Bication lead iodide 2D perovskite component to stabilize inorganic α - CsPbI_3 perovskite phase for high-efficiency solar cells. *Sci Adv* 2017;3:e1700841. [DOI](#) [PubMed](#) [PMC](#)
17. Kim M, Motti SG, Sorrentino R, Petrozza A. Enhanced solar cell stability by hygroscopic polymer passivation of metal halide perovskite thin film. *Energy Environ Sci* 2018;11:2609-19. [DOI](#)
18. Zhang H, Shi J, Zhu L, et al. Polystyrene stabilized perovskite component, grain and microstructure for improved efficiency and stability of planar solar cells. *Nano Energy* 2018;43:383-92. [DOI](#)
19. Yu Y, Tseng C, Chien W, Hsu H, Chen C. Photovoltaic performance enhancement of perovskite solar cells using polyimide and polyamic acid as additives. *J Phys Chem C* 2019;123:23826-33. [DOI](#)
20. Jeong G, Koo D, Seo J, et al. Suppressed interdiffusion and degradation in flexible and transparent metal electrode-based perovskite solar cells with a graphene interlayer. *Nano Lett* 2020;20:3718-27. [DOI](#) [PubMed](#)
21. Yoon J, Kim U, Yoo Y, et al. Foldable perovskite solar cells using carbon nanotube-embedded ultrathin polyimide conductor. *Adv Sci (Weinh)* 2021;8:2004092. [DOI](#) [PubMed](#) [PMC](#)
22. Chen C, Jiang Y, Guo J, et al. Solvent-assisted low-temperature crystallization of SnO_2 electron-transfer layer for high-efficiency planar perovskite solar cells. *Adv Funct Mater* 2019;29:1900557. [DOI](#)
23. Zhang S, Liu Z, Zhang W, et al. Barrier designs in perovskite solar cells for long-term stability. *Adv Energy Mater* 2020;10:2001610. [DOI](#)
24. Wang Q, Dong Q, Li T, Gruverman A, Huang J. Thin insulating tunneling contacts for efficient and water-resistant perovskite solar cells. *Adv Mater* 2016;28:6734-9. [DOI](#) [PubMed](#)
25. Wen X, Wu J, Ye M, Gao D, Lin C. Interface engineering via an insulating polymer for highly efficient and environmentally stable perovskite solar cells. *Chem Commun (Camb)* 2016;52:11355-8. [DOI](#) [PubMed](#)
26. Yang Z, Ma P, Li F, Guo H, Kang C, Gao L. Ultrahigh thermal-stability polyimides with low CTE and required flexibility by formation of hydrogen bonds between poly(amic acids). *European Polymer Journal* 2021;148:110369. [DOI](#)
27. Zhang J, Jiang P, Wang Y, Liu X, Ma J, Tu G. In situ synthesis of ultrastable CsPbBr_3 perovskite nanocrystals coated with polyimide in a CSTR system. *ACS Appl Mater Interfaces* 2020;12:3080-5. [DOI](#) [PubMed](#)
28. Chen N, Yi X, Zhuang J, et al. An efficient trap passivator for perovskite solar cells: poly(propylene glycol) bis(2-aminopropyl ether). *Nanomicro Lett* 2020;12:177. [DOI](#) [PubMed](#) [PMC](#)
29. Huang Z, Hu X, Liu C, et al. Water-resistant and flexible perovskite solar cells via a glued interfacial layer. *Adv Funct Mater* 2019;29:1902629. [DOI](#)
30. Cai Y, Cui J, Chen M, et al. Multifunctional enhancement for highly stable and efficient perovskite solar cells. *Adv Funct Mater* 2021;31:2005776. [DOI](#)
31. Liu K, Liang Q, Qin M, et al. Zwitterionic-surfactant-assisted room-temperature coating of efficient perovskite solar cells. *Joule* 2020;4:2404-25. [DOI](#)
32. Chen C, Li F, Zhu L, et al. Efficient and stable perovskite solar cells thanks to dual functions of oleyl amine-coated $\text{PbSO}_4(\text{PbO})_4$ quantum dots: Defect passivation and moisture/oxygen blocking. *Nano Energy* 2020;68:104313. [DOI](#)
33. Duijnste EA, Ball JM, Le Corre VM, Koster LJA, Snaith HJ, Lim J. Toward understanding space-charge limited current measurements on metal halide perovskites. *ACS Energy Lett* 2020;5:376-84. [DOI](#)
34. Liu Z, Cao F, Wang M, Wang M, Li L. Observing defect passivation of the grain boundary with 2-aminoterephthalic acid for efficient and stable perovskite solar cells. *Angew Chem Int Ed Engl* 2020;59:4161-7. [DOI](#) [PubMed](#)
35. Zhao Y, Zhu P, Huang S, et al. Molecular interaction regulates the performance and longevity of defect passivation for metal halide perovskite solar cells. *J Am Chem Soc* 2020;142:20071-9. [DOI](#) [PubMed](#)
36. Yun S, Ma S, Kwon H, et al. Amino acid salt-driven planar hybrid perovskite solar cells with enhanced humidity stability. *Nano Energy* 2019;59:481-91. [DOI](#)
37. Duan X, Li X, Tan L, et al. Controlling crystal growth via an autonomously longitudinal scaffold for planar perovskite solar cells. *Adv Mater* 2020;32:e2000617. [DOI](#) [PubMed](#)